

Masked Diffusion with Task-awareness for Procedure Planning in Instructional Videos

Fen Fang¹, Yun Liu¹, Ali Koksal¹, Qianli Xu¹, Joo-Hwee Lim^{1,2}

¹Institute for Infocomm Research, Agency for Science, Technology, and Research (A*STAR), Singapore

²Nanyang Technological University, Singapore

1 Fusionopolis Way, #21-01, Connexis (South), Singapore, 138632

Abstract

A key challenge with procedure planning in instructional videos lies in how to handle a large decision space consisting of a multitude of action types that belong to various tasks. To understand real-world video content, an AI agent must proficiently discern these action types (e.g., *pour milk*, *pour water*, *open lid*, *close lid*, etc.) based on brief visual observation. Moreover, it must adeptly capture the intricate semantic relation of the action types and task goals, along with the variable action sequences. Recently, notable progress has been made via the integration of diffusion models and visual representation learning to address the challenge. However, existing models employ rudimentary mechanisms to utilize task information to manage the decision space. To overcome this limitation, we introduce a simple yet effective enhancement - a masked diffusion model. The introduced mask acts akin to a task-oriented attention filter, enabling the diffusion/denoising process to concentrate on a subset of action types. Furthermore, to bolster the accuracy of task classification, we harness more potent visual representation learning techniques. In particular, we learn a joint visual-text embedding, where a text embedding is generated by prompting a pre-trained vision-language model to focus on human actions. We evaluate the method on three public datasets and achieve state-of-the-art performance on multiple metrics. Code is available at <https://github.com/ffzy840304/Masked-PDPP>.

Introduction

Learning procedural knowledge from instructional videos - a natural ability of humans - presents a tough challenge to artificial intelligence (AI). It requires multiple aspects of cognitive and reasoning abilities such as scene understanding, event segmentation and discovery, action recognition and prediction, and causal reasoning (Zhou, Xu, and Corso 2018; Zhou et al. 2023). Building an AI agent with these capabilities is a pressing task for the AI community and has broad implications for real-world applications, e.g., to monitor human behaviors or to assist humans in collaborative tasks. In this paper, we focus on a sub-field of instructional video understanding, namely learning goal-directed actions from real-world videos, and subsequently generate feasible plans. In particular, we follow the work of (Chang et al. 2020) and cast the problem as procedure planning in instructional videos, which requires a model to generate action plans given the visual observations of a start state and a

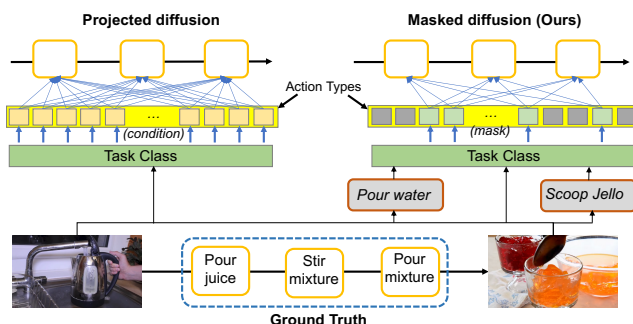


Figure 1: Searching and sorting action sequences from a large set of action types is challenging. Projected diffusion (top left) uses task class as a condition that does not restrict the decision space effectively. We propose masked diffusion (top right) to explicitly manage the decision space. Additionally, text embedding is used to enhance task classification and subsequent action sequence generation.

goal state (an example of *making jello* is illustrated in Figure 1 - bottom). Moreover, we adopt the challenging problem setting of learning with weak supervision, i.e., to learn procedure knowledge without requiring intermediate visual observations (Zhao et al. 2022). Instead, only action labels are provided, which alleviates the costly annotation of the start and end times of each intermediate step.

A key challenge with procedure planning in instructional videos lies in how to handle a large decision space consisting of a multitude of action types that belong to many tasks. For example, there are 778 action types from 180 task classes in the COIN dataset (Tang et al. 2019). Since the datasets are collected from real-world videos at scale, the distribution of actions is largely unknown. In the current problem setting, the visual observations are essentially a pair of images (start and goal states) that are stochastically drawn from a video, and hence it is extremely difficult to recognize them from visual observations. Moreover, planning a sequence of actions from a large pool of actions is even more challenging considering the complicated semantic relationships between action types and task goals. This is exacerbated by the existence of multiple viable action plans to accomplish a specific task goal (Bi, Luo, and Xu 2021).

Early works on procedure planning have employed a

two-branch autoregressive approach while adopting different network architectures to model the probabilistic process. These include the dual dynamics networks (DDN) (Chang et al. 2020), Bayesian Inference using exterior generative adversarial imitation learning (Ext-GAIL) (Bi, Luo, and Xu 2021), and Transformers (Sun et al. 2021). One limitation of these methods is related to the autoregressive process, which is slow and subject to error propagation. Moreover, they require the costly observation of intermediate states as supervisory signals. In contrast, a single-branch non-autoregressive model is proposed that not only simultaneously predicts all intermediate steps, but more importantly alleviates the need for intermediate visual observations (Zhao et al. 2022). However, this method involves a complicated training process on multiple loss functions to manage a large design space. Recently, a diffusion-based probabilistic model is proposed to generate procedure plans non-autoregressively (Wang et al. 2023a). It adopts a two-stage process, namely task classification and action sequence generation. The former aims to capture contextual information and used it as a conditional constraint in the latter step. However, as illustrated in Figure 1 and shown by our results, using the task class as the condition has a limited effect on reducing the design space, *i.e.*, decisions are still made with respect to a large pool of action types.

In this study, we propose a masked diffusion model to use task knowledge as context constraints. Instead of using task labels as a soft condition as in (Wang et al. 2023a), we propose to generate a task-oriented mask to directly restrict the search space of action prediction. As shown in Figure 1, action plans are generated on a greatly reduced subset of action types, owing to the task-guided mask. It helps to reduce the dimensionality of the decision space and enforces stronger hierarchical reasoning. Considering the possible adverse effect of inaccurate task classification, we further enhance visual representation learning via action-aware visual captioning based on pre-trained vision-language models (VLMs). In particular, a text embedding is obtained by prompting a frozen VLM (*e.g.*, LLaVA) (Liu et al. 2023) to focus on the human actions in the current visual scene. We use text-enhanced multimodal embedding to both improve task classification and enhance action planning on the masked diffusion model.

Contributions: (1) We propose a novel masked diffusion model to harness task information and enforce hierarchical procedure planning. Multiple strategies of masking operation are designed and evaluated to show the effectiveness of masking. (2) We enhance visual representation learning with an action-aware text embedding generated from a VLM in a zero-shot manner. We achieve state-of-the-art performance on multiple datasets under different testing conditions. These show the effectiveness of masked diffusion in planning under uncertainty and the potential of text-enhanced representation learning in procedure planning.

Related Work

Action sequence modeling To handle complexities related to a large decision space, early works in procedure planning resort to solutions in probabilistic reasoning for

goal-directed planning, such as universal planning networks (Srinivas et al. 2018), uncertainty-aware action anticipation (Abu Farha and Gall 2019), and causal InfoGAN (Kurutach et al. 2018). However, these models have limited capacity in handling complexities in the scenes of instructional videos. The DDN model (Chang et al. 2020) learns the latent space via the interplay of a transition model and conjugate model, but suffers from compounding error. An Ext-GAIL model is proposed to separately handle time-invariant context knowledge and the casual relationship among actions, where a stochastic model is used to explicitly capture the distribution of plan variants during training (Bi, Luo, and Xu 2021). The PlaTe model adopts transformer-based visual grounding and planning (Sun et al. 2021), but has limited capacity to handle uncertainty. The above approaches suffer from slow convergence and error propagation owing to the auto-regressive reasoning process.

Recently, a memory-enhanced probabilistic procedure planning framework is proposed, which adopts weak and adversarial supervision (Zhao et al. 2022). The method handles uncertainty by combining a pre-trained global memory unit, an adversarial generative model, and a Viterbi post-processing method. However, it involves a complicated training scheme and tedious inference process owing to the computation of multiple loss functions and the brittleness of training GANs. It is also restricted by the limited capability of a small-sized global memory with a fixed structure. The closest work to ours is the projected diffusion procedure planning (PDPP) model (Wang et al. 2023a), which leverages the power of diffusion models to tackle complexity. However, task information is used as a “soft” condition in the representation, resulting in weak guidance to action planning. Moreover, task classification is performed using a simple multilayer perceptron (MLP) on standard visual embedding, which may not fully capture the value of the task context. We anticipate that context/task knowledge is crucial in effective and efficient procedure planning as is shown by numerous empirical evidences in hierarchical procedure planning (Ashutosh et al. 2023; Nair and Finn 2019; Liu et al. 2022; Pertsch et al. 2020).

Visual representation learning Visual reasoning can be enhanced by stronger visual representation learning. In the current problem formulation, the AI agent needs to infer the task type and generate action sequences based solely on two “peeks” into the start and goal states. Recently, notable progress has been made to train and fine-tune large VLMs (Zhao et al. 2023; Xu et al. 2021; Lin et al. 2022; Liu et al. 2023), which is partially driven by the availability of large-scale instructional video datasets (Zhukov et al. 2019; Tang et al. 2019; Damen et al. 2020; Miech et al. 2019; Grauman et al. 2022). The latest models usually use knowledge from the language domain (*e.g.*, wikiHow) as distant supervision signals (Zhong et al. 2023; Zhou et al. 2023; Lin et al. 2022). However, the computational cost of training/fine-tuning large VLMs is usually prohibitively high. Alternatively, efforts have also been made to use pre-trained large language models (LLMs) as a visual planner (Patel et al. 2023; Wang et al. 2023b), leveraging the zero-

shot reasoning ability of powerful foundation models (Ge et al. 2023; Kim et al. 2022; OpenAI 2023; Touvron et al. 2023). However, there is still a notable performance gap due to the lack of domain knowledge. Another stream of research resorts to graph-based representation to capture visual semantics of procedures, ranging from conventional neural task graph (Huang et al. 2019) to sophisticated transformer-based models (Rampášek et al. 2022; Mao et al. 2023; Zhou et al. 2023). One drawback of these models is that they are usually complex with an additional medium of graph representation.

Method

Problem Formulation

Given the visual observations of a start state (o_s) and a goal state (o_g), the procedure planning task is to produce a plan in the form of a sequence of actions $a_{1:T}$ that, when executed, will enable the transition from o_s to o_g in T steps, where T is called the horizon of planning. Similar to (Wang et al. 2023a), we decompose the task into two steps: (1) predicting the task category (e.g., *make sandwich*, *assemble bed*), and (2) generating action sequences conditioned on the predicted task category. The decision process can be formulated as

$$p(a_{1:T}|o_s, o_g) = \int p(a_{1:T}|o_s, o_g, c)p(c|o_s, o_g)dc. \quad (1)$$

The system architecture is shown in Figure 2. As mentioned earlier, using task information as a condition does not exert sufficient modulation power on search space reduction. To address this issue, we propose a new strategy to make use of the task information, namely to generate a mask to restrict the decision space to a subset of “promising” actions. Notably, such a masking approach is different from masked diffusion transformers (Zheng et al. 2023; Gao et al. 2023). The latter aim to strengthen the model’s ability to learn context information for image generation, whereas we use masks to restrict the decision space.

Action-aware Visual Representation Learning

In (Wang et al. 2023a), the task classifier is a simple MLP that takes the concatenated visual embedding of the start and goal state as input. In our model, task class plays an important role in the diffusion process by generating a mask to constrain the design space. Therefore, it is important to improve the accuracy of task classification. We propose two techniques to address this issue. First, we employ a Transformer model (e.g., ViT) (to replace the original MLP) that takes o_s and o_g (based on joint vision-text embedding) to predict the task class (c). Second, we enhance the visual representation by affixing an action-aware text embedding to the visual embedding. It is observed that prevalent image encoders are pre-trained on generic instructional videos, such as Howto100M (Miech et al. 2019), which does not possess sufficient ability to discriminate refined human actions. Fine-tuning such models is both costly and may jeopardize their generalisability. Meanwhile, numerous VLMs have been developed that show impressive descriptive power and flexibility. We adopt LLaVA (Liu et al. 2023) with frozen

network weights¹ and prompt it to concentrate on the human actions in the visual input, e.g., “*Please briefly describe [Image] focusing on the human actions*”. A list of candidate prompts is included in the supplementary material. Despite the explicit request for brevity, the generated description may still be verbose and not suitable for subsequent reasoning. Therefore, we design a simple routine to extract the key words in the form of *verb+noun(s)+[optional]adverb(s)*. For example, in Figure 2, the raw description of the start state can be “*In the image, a person is pouring water into an electric kettle from a faucet.*”. The routine can extract the key information, such as “*pour water into an electric kettle*”. Textual descriptions of o_s and o_g are fed into a pre-trained text encoder to generate the text embedding of the two states. Finally, the text embedding is concatenated with the visual embedding, resulting in the text-enhanced representation (o_s^{VT}, o_g^{VT}).

Masked Diffusion Model

In a standard diffusion model (Ho, Jain, and Abbeel 2020), a forward diffusion process involves incremental addition of Gaussian noise $\epsilon \sim \mathcal{N}(0, \mathbf{I})$ to the input data (x_0 , i.e., the true signal) until it degrades to a random Gaussian distribution x_t . The process is parameterized via a Stochastic Differential Equation (SDE):

$$\begin{aligned} q(x_n, x_0) &= \sqrt{\bar{\alpha}_n}x_0 + \epsilon\sqrt{1 - \bar{\alpha}_n}, \\ q(x_n|x_{n-1}) &= \mathcal{N}(x_n; \sqrt{1 - \beta_n}x_{n-1}, \beta_n\mathbf{I}), \end{aligned} \quad (2)$$

where $\bar{\alpha}_n = \prod_{s=1}^n (1 - \beta_s)$ denotes the noise magnitude, and $\beta_s \in (0, 1)$ specifies the ratio of Gaussian noise added to the signal in each step.

Similarly, the reverse denoising process gradually maps a Gaussian noise into the sample via a discrete SDE:

$$p_\theta(x_{n-1}|x_n) = \mathcal{N}(x_{n-1}; \mu_\theta(x_n, n), \Sigma_\theta(x_n, n)). \quad (3)$$

The network is trained by optimizing the variational lower-bound of $p_\theta(x_0)$, based on which $\Sigma_\theta(x_n, n)$ can be obtained. Meanwhile, $\mu_\theta(x_n, n)$ is reparameterized as a noise prediction network $\epsilon_\theta(x_n, n)$, which is trained with a simple mean-squared error loss $L = \|\epsilon - \epsilon_\theta(x_n, n)\|^2$. After training, the model can recover the signal x_0 from random Gaussian noise.

We construct the input signal by concatenating three elements, namely (1) the text-enhanced visual observations of the start and goal states (o_s^{VT}, o_g^{VT}), (2) the predicted task class (c), and (3) a sequence of candidate actions ($a_{1:T}$), i.e. $x = [(o_s^{VT}, o_g^{VT}), c, a_{1:T}]$. Different from (Wang et al. 2023a), the candidate action sequence is affixed with a binary mask (e.g., ‘1’ for active actions in the predicted task class, ‘0’ for other actions) that is specified by the task class. In practice, the loss function is computed on x with respect to the unmasked actions, x^m . The task-specific mask is derived from the mapping relationship between a task class and the action types, which can be obtained from ground truth during training. In essence, despite the fact that an individual action planning instance does not have the complete list

¹Other VLM models can be used to achieve similar outcome.

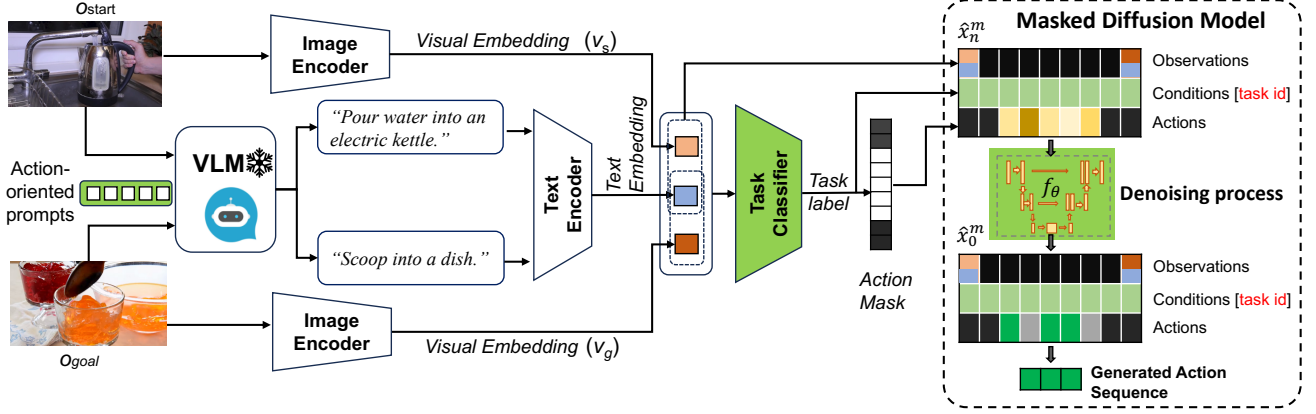


Figure 2: Overview of our masked diffusion model with task-awareness. A frozen Visual-language model (VLM) generates text embedding of the start and goal states based on action-oriented prompts. An action mask is generated based on task class to restrict the action types.

of action types with respect to the task, one can simply include all action types for a specific task from many instances and remove the duplicates.

We adopt a similar condition project scheme on the task class and observations as in (Wang et al. 2023a). Consistent with the premise that the initial and terminal actions are more important due to their primacy and recency effects, additional weights are assigned to these specific actions. The projection operation $Proj()$ in our model is defined as

$$\begin{bmatrix} \hat{c}_1 & \hat{c}_2 & \dots & \hat{c}_T \\ w\hat{a}_1^m & \hat{a}_2^m & \dots & w\hat{a}_T^m \\ \hat{o}_1 & \hat{o}_2 & \dots & \hat{o}_T \end{bmatrix} \rightarrow \begin{bmatrix} c & c & \dots & c \\ w\hat{a}_1^m & \hat{a}_2^m & \dots & w\hat{a}_T^m \\ o_s^{VT} & 0 & \dots & o_g^{VT} \end{bmatrix}, \quad (4)$$

x^m $Proj(x^m)$

where \hat{c}_i , \hat{o}_i and \hat{a}_i^m refer to the i^{th} horizon task class, observation dimensions and predicted masked action logits in masked representation x^m , respectively. c , o_s^{VT} , o_g^{VT} represent the specified conditions.

The projection operation in Eq. 4 indicates that the guidance is not changed during training. More importantly, after projecting task classification and observations to their original values, the loss on x^m is exclusively attributed to a^m . Thus, the training loss can be computed as follows:

$$\mathcal{L}_{diff}^m = \sum_{n=1}^N (\epsilon_{\theta}(a_n^m, n) - a_0^m)^2. \quad (5)$$

By employing a binary mask on the action dimensions, Gaussian noise is exclusively introduced to unmasked active actions. As a result, the search space for optimal actions is confined to the task-defined subset, rather than encompassing the entire action space of the dataset. This operation considerably reduces the learning load of the model during loss minimization, which in turn leads to a streamlined convergence process and enhanced accuracy in the denoising phase. This benefit becomes even more pronounced as the action space becomes larger.

Algorithm 1: Training Process

-
- Input:** Initial input x_0 , Gt task class c , the condition project function $Proj()$, total diffusion steps N , diffusion model ϵ_{θ} , $\{\bar{\alpha}_n\}_{n=1}^N$
- 1: apply a binary mask to action dimension in x_0 given c
 - 2: $a_0^m = a_0[0, 1, 0 \dots 1, 0]$ (a in c value is ‘1’, otherwise ‘0’)
 - 3: **repeat**
 - 4: $n \sim \{1, N\}$
 - 5: $\epsilon \sim \mathcal{N}(0, \mathbf{I})$
 - 6: $x_n^m = \sqrt{\bar{\alpha}_n}x_0^m + \epsilon\sqrt{1 - \bar{\alpha}_n}$
 - 7: $\hat{x}_0^m = \epsilon_{\theta}(Proj(x_n^m), n)$
 - 8: **Take gradient descent step on**
 - 9: $\nabla_{\theta} \|x_0^m - Proj(\hat{x}_0^m)\|^2$
 - 10: **until** converged
-

Training

Our training program consists of two main stages: (1) training of a task class prediction model to extract conditional guidance from start to goal observation as well as action masks; (2) leveraging the masked diffusion model to effectively fit the target action sequence distribution.

As mentioned earlier, a binary mask is applied to the action dimensions, directing the denoising model to focus on active actions. In the action sequence distribution fitting stage, we adopt the U-Net architecture (Ronneberger, Fischer, and Brox 2015) to learn the noise prediction model $\epsilon_{\theta}(x_n, n)$ on the masked action distribution, as it resembles the stacked denoising autoencoders. By minimizing \mathcal{L}_{diff}^m , the model effectively mitigates the impact of randomly introduced noise on x_n^m . The detailed denoising model training process is shown in Algorithm 1.

Inference

During the inference stage, only the initial observation o_s and the target observation o_g are given. The task class is generated through the trained task classifier, eliminating the need for the ground truth task class as in the training phase. Subsequently, Gaussian noise is introduced to the conditions

Algorithm 2: Inference Process

Input: Total diffusion steps N , task class prediction c , model ϵ_θ , $\{\bar{\alpha}_n\}_{n=1}^N$, $\{\beta_n\}_{n=1}^N$
1: apply a binary mask to action dimension in \hat{x}_N given c
2: $\hat{a}_N^m = \hat{a}_N[0, 1, 0 \dots 1, 0]$ (a in c value is ‘1’, otherwise ‘0’)
3: **for** $n = N, \dots, 1$ **do**
4: $\hat{x}_n^m = \epsilon_\theta(\text{Proj}(x_n^m), n)$
5: **if** $n > 1$ **then**
6: $\hat{\mu}_n = \frac{\sqrt{\bar{\alpha}_{n-1}\beta_n}}{1-\bar{\alpha}_n}\hat{x}_0^m + \frac{\sqrt{\bar{\alpha}_n(1-\bar{\alpha}_{n-1})}}{1-\bar{\alpha}_n}\hat{x}_n^m$
7: $\hat{\Sigma}_n = \frac{1-\bar{\alpha}_{n-1}}{1-\bar{\alpha}_n} \cdot \beta_n$
8: $\hat{x}_{n-1}^m \sim \mathcal{N}(\hat{x}_{n-1}^m; \hat{\mu}_n, \hat{\Sigma}_n \mathbf{I})$
9: **end if**
10: **end for**
11: return \hat{x}_0^m

of the observations and masked action dimensions, resulting in the creation of x_n^m . The acquired denoise model is then employed to conduct denoising N times for sampling an optimal action sequence. The detailed procedure in the inference stage is shown in Algorithm 2.

Implementation Details

The perceptual input to our model is a 1536-dimensional vector that represents the visual features extracted from HowTo100M (Miech et al. 2019). For the text representation input, we utilize LLaVa’s (Liu et al. 2023) prompt-extracted text, which is subsequently encoded into a 578-dimensional vector using a DistilBERT (Sanh et al. 2019) base model. All models are trained using a linear warm-up scheme. Throughout our experiments, the training batch size remains constant at 256. All the experiments are conducted using the ADAM optimizer (Kingma and Ba 2014) on a setup consisting of 4 NVIDIA RTX A5000 GPUs. Refer to supplement for more detailed information, such as learning rate and training epochs on different datasets.

Experiments

Evaluation Protocol

Datasets We conduct evaluations of our model on three instructional video datasets: CrossTask (Zhukov et al. 2019), NIV (Alayrac et al. 2016), and COIN (Tang et al. 2019). The CrossTask dataset comprises 2,750 videos spanning 18 different tasks, with an average of 7.6 actions per video. The NIV dataset consists of 150 videos depicting 5 daily tasks, with an average of 9.5 actions per video. The COIN dataset contains 11,827 videos involving 180 different tasks, with an average of 3.6 actions per video. We adopt the standard approach by randomly splitting the data, using 70% for training and 30% for testing (Zhao et al. 2022; Sun et al. 2021; Wang et al. 2023a). We adhere to the data pre-processing methodology (Wang et al. 2023a) to generate action sequences and select {start, goal} observations.

Metrics In accordance with prior studies (Zhao et al. 2022; Sun et al. 2021; Wang et al. 2023a), we employ three

metrics to assess the performance of our approach: (1) *Success Rate (SR)*: A plan is considered correct only if all actions in the predicted sequence exactly match the corresponding actions in the ground truth. (2) *Mean Accuracy (mAcc)*: It is the accuracy of actions at each individual time step. An action is considered correct if it precisely matches the action in the ground truth at the same time step. (3) *Mean Intersection over Union (mIoU)*: It quantifies the overlap between predicted actions and the ground truth by computing the action IoU. Note that *mIoU* does not consider the order of actions and solely indicates whether the model effectively captures the correct set of steps required to complete the procedure plan. Following (Wang et al. 2023a), we calculate the *mIoU* metric on each individual sequence, instead of computing it on every mini-batch, as done in prior studies (Zhao et al. 2022; Sun et al. 2021). This is a more stringent condition and allows us to assess the accuracy of predicted actions for each specific sequence independently.

In addition, we conduct a comprehensive evaluation of the stochastic nature of our model by employing various probabilistic metrics: (1) *Kullback–Leibler divergence (KL-Div)* and *Negative Log Likelihood (NLL)* between the probability distributions of the predicted plans and the corresponding ground truth; (2) *Mode Recall (ModeRec)* to assess the coverage of ground truth modes in the results, and (3) *Mode Precision (ModePrec)* to indicate the frequency with which our predicted plans align with the true modes of the data.

Baselines We include recent procedure planning approaches based on instructional videos as baselines (Chang et al. 2020; Sun et al. 2021; Bi, Luo, and Xu 2021; Zhao et al. 2022; Wang et al. 2023a).

Task Classification Results

We intend to improve the task prediction accuracy by employing a combination of visual and text representations along with a transformer model. The results of task prediction performance are shown in Table 1, where different configurations are examined. Our model achieves an improvement of approximately 3% in task classification accuracy on the COIN dataset (with the largest task space). It achieves a slight improvement on CrossTask; and maintains perfect accuracy (100%) on NIV as in other configurations.

To verify the influence of task classification on the ultimate accuracy of action planning, we compare the outcomes achieved through the utilization of the MLP as detailed in (Wang et al. 2023a) with the results obtained by incorporating Transformer classifiers as inputs for both PDPP and our model. We observe a positive effect of Transformer, as shown by the results in supplementary section D.

Comparison with Prior Approaches

Crosstask (short horizon) We show the main performance results on CrossTask in Table 2. Our model consistently outperforms other approaches in terms of both *SR* and *mAcc*. Across sequence lengths $T = 3$ and 4, our model exhibits a notable *SR* increase of approximately 2% (absolute change) compared to the previous state-of-the-art (SotA). In

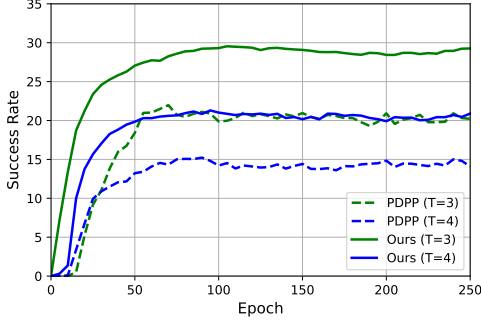


Figure 3: Success rate during training on COIN dataset.

terms of $mAcc$, our model showcases significant enhancements, achieving more than 11% improvement at $T = 3$ and around 2.3% at $T = 4$. Regarding $mIoU$, as aforementioned, we follow PDPP (Wang et al. 2023a) to compute it by calculating the mean of every IoU for a single action sequence rather than a mini-batch adopted by (Sun et al. 2021; Zhao et al. 2022). Hence, a direct comparison with (Sun et al. 2021; Zhao et al. 2022) is not relevant. Compared to PDPP, our model achieves about 1.5% improvement in $mIoU$.

CrossTask (long horizon) Following (Zhao et al. 2022; Wang et al. 2023b), we evaluate the performance on predicting plans for longer time horizons, $T = 3, 4, 5, 6$. The results are shown in Table 3. Our model consistently achieves substantial enhancements across all planning horizons, surpassing the performance of previous models.

NIV and COIN Results on the NIV and COIN datasets are presented in Table 4. It is shown that our method demonstrates superior performance on both datasets, surpassing other approaches in terms of SR and $mAcc$ metrics. In particular, on the relatively smaller NIV dataset, our model achieves 1% ($T = 3$) and 2% ($T = 4$) increases respectively in SR , along with improvements of 0.6% ($T = 3$) and 1.3% ($T = 4$) in $mAcc$. On the COIN dataset, which poses the highest level of difficulty, our method achieves a remarkable absolute improvement of 8.1% ($T = 3$) and 6.9% ($T = 4$) on SR , and 4% ($T = 3$) and 2.7% ($T = 4$) on $mAcc$ metrics, respectively. These represent a substantial margin over previous SotA, *i.e.*, PDPP. Such a performance boost is also illustrated in Figure 3, which shows the training process on COIN dataset. Our approach features a large margin on SR and a faster learning speed, especially during the initial stage of training.

Evaluating Probabilistic Modeling

To assess the effectiveness of our method on probabilistic modeling, we conduct a comparison between the plan distributions generated by our model and the ground truth distribution of viable plans, following the protocol proposed in (Zhao et al. 2022; Wang et al. 2023a). The evaluation is done on CrossTask dataset which is most suitable for this purpose with its higher variations in feasible plans. Results on NIV and COIN datasets are included in the supplementary material. We compare our model with three baselines:

Table 1: Task classification results. VM: visual representation + MLP classifier; VTM: visual-text representation + MLP classifier; VTT: visual-text representation + Transformer classifier.

	CrossTask				COIN		NIV	
	$T=3$	$T=4$	$T=5$	$T=6$	$T=3$	$T=4$	$T=3$	$T=4$
VM	92.4	93.0	93.4	93.2	79.4	78.9	100	100
VTM	92.7	93.2	93.5	93.6	81.0	80.2	100	100
VTT	92.9	93.3	93.8	93.7	82.6	81.9	100	100

(1) a Deterministic baseline established by setting the initial distribution $\hat{x}_N = 0$, (2) a Noise baseline achieved by directly sampling from a random distribution using the provided observations and task class condition in a single step, and (3) the original PDPP approach (Wang et al. 2023a).

The outcomes are presented in Table 5. Our model consistently produces the lowest NLL and $KL-Div$ values across all horizons in comparison with the other three models. The results underscore the enhanced proficiency of our model in managing uncertainty. Furthermore, our model exhibits a remarkable capability to generate plans that are both diverse and logical, consistently outperforming the other models in terms of SR , $ModePrec$, and $ModeRec$ across all horizons.

Ablation Studies

Effect of text-enhanced representation learning To validate the efficacy of text-enhanced representation learning within our model, we compare the performance of three setups: (1) the original PDPP model that utilizes only visual representation, (2) a truncated model that uses only text-based representation, and (3) a model that employs joint vision-text representations. The results are listed in Table 6. Apparently, the text-only modality is inferior to the visual-only modality and the vision-text multimodality in representation learning. Importantly, the additional action-aware text embedding does have a positive effect on planning efficacy as indicated by the higher performance of vision-text joint representation than visual-only. This outcome is consistent with the information in Table 1, wherein higher accuracy of task classification is achieved when vision-text joint representation is used.

Effect of masked diffusion We conduct an ablation study to investigate the impact of different masking techniques on performance. In our method, we apply a binary mask to the action dimensions (called hard mask). Gaussian noise is exclusively generated within the unmasked regions, corresponding to the actions relevant to the active task. However, a possible adverse effect is that if the task classification is incorrect, there is a substantial likelihood that the action plans are wrong. Hence, we use the confidence score of task prediction to dictate the likelihood of a set of actions being retained, enabling the creation of a “soft” mask that is applied to the action dimensions. We also include a condition where no masking is applied to the action dimensions (w/o mask), resulting in a diffusion model identical to that of PDPP.

The SR results are outlined in Table 7 - detailed data for SR , $mAcc$, and $mIoU$ can be found in supplementary ma-

Table 2: Performance of benchmarks with planning horizons $T \in \{3, 4\}$ on CrossTask. The ‘Supervision’ column indicates the type of supervision during training. ‘V’: intermediate visual states; ‘L’: language features; ‘C’: task class. Notably, to get *mIoU*, we compute the average IoU for each individual action sequence, rather than across a mini-batch (in grey font).

Models	Supervision	$T=3$			$T=4$		
		SR \uparrow	mAcc \uparrow	mIoU \uparrow	SR \uparrow	mAcc \uparrow	mIoU \uparrow
DDN (Chang et al. 2020)	V	12.18	31.29	47.48	5.97	27.10	48.46
PlaTe (Sun et al. 2021)	L	16.00	36.17	65.91	14.00	35.29	44.36
Ext-GAIL (Bi, Luo, and Xu 2021)	V	21.27	49.46	61.70	16.41	43.05	60.93
P ³ IV (Zhao et al. 2022)	L	23.34	49.46	73.89	13.40	44.16	70.01
PDPP (Wang et al. 2023a)	C	37.20	55.35	66.57	21.48	57.82	65.13
Ours	C	39.17	66.66	68.31	23.47	60.16	66.75

Table 3: Results of success rate for longer planning horizons on CrossTask.

Models	$T=3$	$T=4$	$T=5$	$T=6$
	SR \uparrow	SR \uparrow	SR \uparrow	SR \uparrow
DDN (Chang et al. 2020)	12.18	5.97	3.10	1.20
PlaTe (Sun et al. 2021)	18.50	14.00	10.00	7.50
P ³ IV (Zhao et al. 2022)	23.34	13.40	7.21	4.40
PPDP (Wang et al. 2023a)	37.20	21.48	13.58	8.47
Ours	39.17	23.47	15.25	10.10

Table 4: Results for prediction horizons $T \in \{3, 4\}$ on NIV and COIN datasets. ‘Sup.’ means the type of supervision during training.

Hor.	Models	Sup.	NIV			COIN		
			SR \uparrow	mAcc \uparrow	mIoU \uparrow	SR \uparrow	mAcc \uparrow	mIoU \uparrow
$T=3$	DDN	V	18.41	32.54	56.56	13.9	20.19	64.78
	Ext-GAIL	V	22.11	42.20	65.93	-	-	-
	P ³ IV	L	24.68	49.01	74.29	15.4	21.67	76.31
	PDPP	C	31.25	49.26	57.92	21.33	45.62	51.82
	Ours	C	32.35	49.89	58.90	29.43	49.50	52.20
$T=4$	DDN	V	15.97	27.09	53.84	11.13	17.71	68.06
	Ext-GAIL	V	19.91	36.31	53.84	-	-	-
	P ³ IV	L	20.14	38.36	67.29	11.32	18.85	70.53
	PDPP	C	26.72	48.92	59.04	14.41	44.10	51.39
	Ours	C	28.88	50.20	59.75	21.30	46.84	52.45

Table 5: Uncertainty and diversity evaluation on CrossTask.

Hori.	Model	NLL \downarrow	KL-Div \downarrow	SR \uparrow	ModePrec \uparrow	ModeRec \uparrow
$T=3$	Deterministic	3.57	2.99	39.03	55.60	34.13
	Noise	3.58	3.00	34.92	51.04	39.42
	PDPP	3.61	3.03	37.20	53.14	36.49
	Ours	3.10	2.52	39.17	56.03	44.52
$T=4$	Deterministic	4.29	3.40	21.17	45.65	18.35
	Noise	4.04	3.15	18.99	43.90	25.56
	PDPP	3.85	2.96	21.28	44.55	31.10
	Ours	3.41	2.52	23.47	47.33	34.60
$T=5$	Deterministic	4.70	3.54	12.59	35.47	11.20
	Noise	4.45	3.30	12.04	34.35	15.67
	PDPP	3.77	2.62	13.58	36.30	29.45
	Ours	3.61	2.46	15.25	36.56	30.12
$T=6$	Deterministic	5.12	3.82	7.47	25.24	6.75
	Noise	4.97	3.49	7.82	24.51	11.04
	PDPP	4.06	2.76	8.47	25.61	22.68
	Ours	3.67	2.37	10.10	25.90	28.69

terials. It is shown that hard masking results in the highest *SR*. In fact, even without applying masking to action dimensions, the ‘w/o mask’ configuration outperforms PDPP, possibly due to improved task class prediction facilitated by text-enhanced representation. Interestingly, soft masking leads to the lowest *SR*, performing worse than both PDPP

Table 6: Ablation study on the role of text-enhanced representation learning.

Models	CrossTask				NIV		COIN	
	$T=3$	$T=4$	$T=5$	$T=6$	$T=3$	$T=4$	$T=3$	$T=4$
PDPP(V)	37.20	21.48	13.58	8.47	31.25	26.72	21.33	14.41
PDPP(T)	32.18	18.86	11.47	8.15	28.33	24.87	17.63	11.35
PDPP(V+T)	37.72	22.07	14.03	9.04	31.73	27.41	24.46	16.02

Table 7: Ablation study on the role of the masking type.

	CrossTask				NIV		COIN	
	$T=3$	$T=4$	$T=5$	$T=6$	$T=3$	$T=4$	$T=3$	$T=4$
PDPP	37.20	21.48	13.58	8.47	31.25	26.72	21.33	14.41
w/o mask	37.72	22.07	14.03	9.04	31.73	27.41	24.46	16.02
Soft mask	34.37	18.44	12.04	7.73	30.44	26.07	18.76	12.57
Hard mask	39.17	23.47	15.25	10.10	32.35	28.88	27.85	20.24

and the non-masked approach. The possible reason is that with hard masking, action planning is confined within the boundaries of a task. This restriction significantly reduces the action space, allowing for a thorough exploration of the action sequencing within the unmasked subset of actions. With soft masking, the confidence scores of task classification could be ill-calibrated (Guo et al. 2017), which leads to wrong allocation to task-guided action types.

Conclusion

In this paper, we have introduced a masked diffusion model to deal with the large design space that challenges procedure planning in instructional videos. A simple yet effective masking mechanism is designed in a projected diffusion model to restrict the scope of planning to a subset of actions, as is guided by the task class information. We show that such a binary mask leads to significant improvements in procedure planning with respect to multiple metrics. It also engenders a positive effect on probabilistic modeling to reflect the inherent data distribution. Furthermore, we show the preferable effect of text-enhanced representation learning, which leverages the power of large VLMs and generates action-aware text description simply via prompting, without the need for computationally intensive training or fine-tuning. A direction of future work is to develop a more sophisticated masking scheme based on a well-calibrated task prediction model, so as to allow for a well-balanced compromise between the reduction in dimensions induced by masking and the retention of context relevant to the task.

References

- Abu Farha, Y.; and Gall, J. 2019. Uncertainty-Aware Anticipation of Activities. In *IEEE/CVF International Conference on Computer Vision Workshops*, 1197–1204.
- Alayrac, J.-B.; Bojanowski, P.; Agrawal, N.; Sivic, J.; Laptev, I.; and Lacoste-Julien, S. 2016. Unsupervised Learning from Narrated Instruction Videos. In *IEEE Conference on Computer Vision and Pattern Recognition*, 4575–4583.
- Ashutosh, K.; Girdhar, R.; Torresani, L.; and Grauman, K. 2023. HierVL: Learning Hierarchical Video-Language Embeddings. In *IEEE/CVF Conference on Computer Vision and Pattern Recognition*, 23066–23078.
- Bi, J.; Luo, J.; and Xu, C. 2021. Procedure Planning in Instructional Videos via Contextual Modeling and Model-based Policy Learning. In *IEEE/CVF International Conference on Computer Vision*, 15591–15600.
- Chang, C.-Y.; Huang, D.-A.; Xu, D.; Adeli, E.; Fei-Fei, L.; and Niebles, J. C. 2020. Procedure planning in instructional videos. In *European Conference on Computer Vision*, 334–350.
- Damen, D.; Doughty, H.; Farinella, G. M.; Furnari, A.; Kazakos, E.; Ma, J.; Moltisanti, D.; Munro, J.; Perrett, T.; Price, W.; and Wray, M. 2020. Rescaling Egocentric Vision: Collection, Pipeline and Challenges for EPIC-KITCHENS-100. *International Journal of Computer Vision*, 130: 33–55.
- Gao, S.; Zhou, P.; Cheng, M.-M.; and Yan, S. 2023. Masked Diffusion Transformer is a Strong Image Synthesizer. *ArXiv*, abs/2303.14389.
- Ge, J.; Luo, H.; Qian, S.; Gan, Y.; Fu, J.; and Zhang, S. 2023. Chain of Thought Prompt Tuning in Vision Language Models. *ArXiv*, abs/2304.07919.
- Grauman, K.; Westbury, A.; Byrne, E.; and et al. 2022. Ego4D: Around the World in 3,000 Hours of Egocentric Video. *IEEE/CVF Conference on Computer Vision and Pattern Recognition*, 18973–18990.
- Guo, C.; Pleiss, G.; Sun, Y.; and Weinberger, K. Q. 2017. On Calibration of Modern Neural Networks. In *International Conference on Machine Learning*.
- Ho, J.; Jain, A.; and Abbeel, P. 2020. Denoising Diffusion Probabilistic Models. In *Advances in Neural Information Processing Systems*, 6840–6851.
- Huang, D.-A.; Nair, S.; Xu, D.; Zhu, Y.; Garg, A.; Fei-Fei, L.; Savarese, S.; and Niebles, J. C. 2019. Neural Task Graphs: Generalizing to Unseen Tasks From a Single Video Demonstration. In *IEEE/CVF Conference on Computer Vision and Pattern Recognition*, 8557–8566.
- Kim, J.; Nguyen, D.; Min, S.; Cho, S.; Lee, M.; Lee, H.; and Hong, S. 2022. Pure Transformers are Powerful Graph Learners. In *Advances in Neural Information Processing Systems*, 14582–14595.
- Kingma, D.; and Ba, J. 2014. Adam: A Method for Stochastic Optimization. *International Conference on Learning Representations*.
- Kurutach, T.; Tamar, A.; Yang, G.; Russell, S. J.; and Abbeel, P. 2018. Learning Plannable Representations with Causal InfoGAN. In *Advances in Neural Information Processing Systems*, 8747–8758.
- Lin, X.; Petroni, F.; Bertasius, G.; Rohrbach, M.; Chang, S.-F.; and Torresani, L. 2022. Learning To Recognize Procedural Activities with Distant Supervision. *IEEE/CVF Conference on Computer Vision and Pattern Recognition*, 13843–13853.
- Liu, A.; Sohn, S.; Qazwini, M.; and Lee, H. 2022. Learning Parameterized Task Structure for Generalization to Unseen Entities. In *AAAI Conference on Artificial Intelligence*, 7534–7541.
- Liu, H.; Li, C.; Wu, Q.; and Lee, Y. J. 2023. Visual Instruction Tuning. *ArXiv*, abs/2304.08485.
- Mao, W.; Desai, R.; Iuzzolino, M. L.; and Kamra, N. 2023. Action Dynamics Task Graphs for Learning Plannable Representations of Procedural Tasks. *ArXiv*, abs/2302.05330.
- Miech, A.; Zhukov, D.; Alayrac, J.-B.; Tapaswi, M.; Laptev, I.; and Sivic, J. 2019. HowTo100M: Learning a Text-Video Embedding by Watching Hundred Million Narrated Video Clips. In *IEEE/CVF International Conference on Computer Vision*, 2630–2640.
- Nair, S.; and Finn, C. 2019. Hierarchical Foresight: Self-Supervised Learning of Long-Horizon Tasks via Visual Subgoal Generation. *ArXiv*, abs/1909.05829.
- OpenAI. 2023. GPT-4 Technical Report. *ArXiv*, abs/2303.08774.
- Patel, D.; Eghbalzadeh, H.; Kamra, N.; Iuzzolino, M. L.; Jain, U.; and Desai, R. 2023. Pretrained Language Models as Visual Planners for Human Assistance. *ArXiv*, abs/2304.09179.
- Pertsch, K.; Rybkin, O.; Ebert, F.; Zhou, S.; Jayaraman, D.; Finn, C.; and Levine, S. 2020. Long-Horizon Visual Planning with Goal-Conditioned Hierarchical Predictors. In *Advances in Neural Information Processing Systems*, 17321–17333.
- Rampásek, L.; Galkin, M.; Dwivedi, V. P.; Luu, A. T.; Wolf, G.; and Beaini, D. 2022. Recipe for a General, Powerful, Scalable Graph Transformer. In *Advances in Neural Information Processing Systems*, 14501–14515.
- Ronneberger, O.; Fischer, P.; and Brox, T. 2015. U-Net: Convolutional Networks for Biomedical Image Segmentation. In *International Conference on Medical Image Computing and Computer-Assisted Intervention*, 234–241.
- Sanh, V.; Debut, L.; Chaumond, J.; and Wolf, T. 2019. DistilBERT, a distilled version of BERT: smaller, faster, cheaper and lighter. *ArXiv*, abs/1910.01108.
- Srinivas, A.; Jabri, A.; Abbeel, P.; Levine, S.; and Finn, C. 2018. Universal Planning Networks: Learning Generalizable Representations for Visuomotor Control. In *International Conference on Machine Learning*, 4732–4741.
- Sun, J.; Huang, D.-A.; Lu, B.; Liu, Y.; Zhou, B.; and Garg, A. 2021. PlaTe: Visually-Grounded Planning With Transformers in Procedural Tasks. *IEEE Robotics and Automation Letters*, 7: 4924–4930.
- Tang, Y.; Ding, D.; Rao, Y.; Zheng, Y.; Zhang, D.; Zhao, L.; Lu, J.; and Zhou, J. 2019. COIN: A Large-Scale Dataset for

Comprehensive Instructional Video Analysis. In *IEEE/CVF Conference on Computer Vision and Pattern Recognition*, 1207–1216.

Touvron, H.; Lavril, T.; Izacard, G.; Martinet, X.; Lachaux, M.-A.; Lacroix, T.; Rozière, B.; Goyal, N.; Hambro, E.; Azhar, F.; Rodriguez, A.; Joulin, A.; Grave, E.; and Lample, G. 2023. LLaMA: Open and Efficient Foundation Language Models. *ArXiv*, abs/2302.13971.

Wang, H.; Wu, Y.; Guo, S.; and Wang, L. 2023a. PDPP: Projected Diffusion for Procedure Planning in Instructional Videos. In *IEEE/CVF Conference on Computer Vision and Pattern Recognition*, 14836–14845.

Wang, Q.; Li, M.; Chan, H. P.; Huang, L.; Hockenmaier, J.; Chowdhary, G. V.; and Ji, H. 2023b. Multimedia Generative Script Learning for Task Planning. In *Annual Meeting of the Association for Computational Linguistics*, 986–1008.

Xu, H.; Ghosh, G.; Huang, P.-Y. B.; Okhonko, D.; Aghajanyan, A.; and Feichtenhofer, F. M. L. Z. C. 2021. Video-CLIP: Contrastive Pre-training for Zero-shot Video-Text Understanding. In *Conference on Empirical Methods in Natural Language Processing*, 6787–6800.

Zhao, H.; Hadji, I.; Dvornik, N.; Derpanis, K. G.; Wildes, R. P.; and Jepson, A. D. 2022. P3IV: Probabilistic Procedure Planning from Instructional Videos with Weak Supervision. In *IEEE/CVF Conference on Computer Vision and Pattern Recognition*, 2928–2938.

Zhao, Y.; Misra, I.; Krähenbühl, P.; and Girdhar, R. 2023. Learning Video Representations from Large Language Models. In *IEEE/CVF Conference on Computer Vision and Pattern Recognition*, 6586–6597.

Zheng, H.; Nie, W.; Vahdat, A.; and Anandkumar, A. 2023. Fast Training of Diffusion Models with Masked Transformers. *ArXiv*, abs/2306.09305.

Zhong, Y.; Yu, L.; Bai, Y.; Li, S.; Yan, X.; and Li, Y. 2023. Learning Procedure-aware Video Representation from Instructional Videos and Their Narrations. In *IEEE/CVF Conference on Computer Vision and Pattern Recognition*, 14825–14835.

Zhou, H.; Martín-Martín, R.; Kapadia, M.; Savarese, S.; and Niebles, J. C. 2023. Procedure-Aware Pretraining for Instructional Video Understanding. In *IEEE/CVF Conference on Computer Vision and Pattern Recognition*, 10727–10738.

Zhou, L.; Xu, C.; and Corso, J. 2018. Towards Automatic Learning of Procedures from Web Instructional Videos. In *AAAI Conference on Artificial Intelligence*, 7590–7598.

Zhukov, D.; Alayrac, J.-B.; Cinbis, R. G.; Fouhey, D.; Laptev, I.; and Sivic, J. 2019. Cross-task Weakly Supervised Learning from Instructional Videos. In *IEEE/CVF Conference on Computer Vision and Pattern Recognition*, 3537–3545.

Supplementary Material for “Masked Diffusion with Task-awareness for Procedure Planning in Instructional Videos”

Written by AAI Press Staff^{1*}

AAAI Style Contributions by Pater Patel Schneider, Sunil Issar,
J. Scott Penberthy, George Ferguson, Hans Guesgen, Francisco Cruz[†], Marc Pujol-Gonzalez[†]

¹Association for the Advancement of Artificial Intelligence
1900 Embarcadero Road, Suite 101
Palo Alto, California 94303-3310 USA
proceedings-questions@aaai.org

Supplementary Material Overview

This supplementary material consists of the following contents. (1) In Sec. A, we provide the details of sub-models, including the task classification model at the first training stage and the diffusion model at the second stage. (2) In Sec. B, we describe the detailed baselines. (3) In Sec. C, we show the performance comparison using an alternative protocol on the CrossTask dataset (?). (4) In Sec. D, we present a comparison of the success rates in action planning on the COIN dataset (?). We utilize various task classifiers to showcase the influence of task classification on the overall accuracy of the final action planning process. (5) In Sec. E, to demonstrate how the masking scheme facilitate decision making at varying sizes of the search space, we compare the performance gap between our model and PDPP on subsets of COIN that include different numbers of tasks (and hence action types). (6) In Sec. F, we provide more results on how our model handle uncertainty. (7) In Sec. G, we provide a list of prompts designed for the LLaVA model (?). Additionally, we showcase textual descriptions of images generated by the visual-language model.

A. Details of the sub-models in our method

A.1 Transformer classifier In the phase of task classification learning, we replace the MLP model (?) with a Transformer, namely the ViT architecture (?). Our approach leverages visual representations denoted as a 1536-dimensional feature vector and text representations denoted as a 768-dimensional vector for both start and goal observations. To configure the input for the ViT model, we amalgamate two text representations into a single 1536-dimensional feature. This combined feature is then triplicated and concatenated to create a 3-channel input, denoted as a 3×1536 -dimensional feature array. These features are subsequently molded into a $3 \times 48 \times 32$ arrangement, optimally priming them for input into the ViT model. Fig. 1 gives a visual illustration of this procedure.

A.2 Detail of diffusion model - U-Net We employ the popular U-Net (?) architecture as the base diffusion model.

*With help from the AAI Publications Committee.

[†]These authors contributed equally.

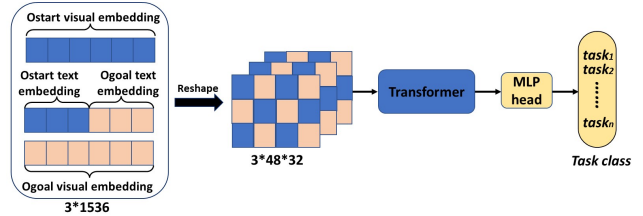


Figure 1: Task classifier architecture.

Such an architecture resembles the stacked denoising autoencoders. Considering that the value of planning horizon is small ($T = \{3, 4, 5, 6\}$), the U-Net is set as 3 layers. We configure the 1D-convolutional kernel with a size of 2, a stride of 1, and padding set to 0. This arrangement ensures that the length of the planning horizon dimension remains constant at 1 after each downsampling or upsampling operation.

The input to the diffusion model comprises the concatenation of task class, action labels, and observation features (including visual and text). As a result, the size of the feature dimension is denoted as $dim = L_c + L_a + L_o$, where L_c refers to the number of task classes present in the dataset, L_a represents the number of distinct actions within the dataset, and L_o corresponds to the length of visual features. The feature dimensions in the three layers of the downsampling process evolve as follows: $256 \rightarrow 512 \rightarrow 1024$. Conversely, in the upsampling process, the dimension transition is specified as $1024 \rightarrow 512 \rightarrow 256$, ultimately restoring to the initial dimension, dim .

A.3 Details of training process

We employ a linear warm-up scheme during training, with slightly different settings to accommodate characteristics of individual datasets.

For the CrossTask dataset (?), we configure a diffusion step value of 200. Our model undergoes a training process spanning 24,000 steps, with the learning rate progressively increasing linearly up to $5e-4$ within the initial 4,000 steps. Subsequently, the learning rate undergoes a decay of 0.5 at

the 10,000th, 16,000th, and 22,000th steps.

The NIV dataset (?) is characterized by its smaller size. We set a diffusion step value of 50. The training duration spans 6,500 steps, during which the learning rate follows a linear increase up to $3e-4$ for the first 4,500 steps, followed by a 0.5 decay at step 6,000.

For the COIN dataset (?), we adopt a more extensive training regime due to its larger scale. We establish a diffusion step of 200 and a training duration of 160,000 steps. The learning rate commences with a linear increase to $1e-5$ over the initial 4,000 steps, followed by 0.5 decay at the 14,000th and 24,000th steps. Subsequently, the learning rate is kept constant at $2.5e-6$ for the remaining training iterations.

In all experimental setups, the training batch size is set at 256. Our training process incorporates a weighted loss mechanism with a weight parameter (w) set to 10. All experiments are conducted utilizing the ADAM optimization algorithm (?) on a setup involving 4 NVIDIA RTX A5000 GPUs.

B. Baselines

In this section, we present the baselines employed in our paper.

- *DDN* (?). The DDN model comprises a dual-branch autoregressive structure, which is designed to acquire a conceptual representation of action steps and endeavors to prognosticate state-action transitions within the feature space.
- *PlaTe* (?). The PlaTe model, similar to DDN, employs transformer modules in a dual-branch setup to facilitate its prediction process.
- *Ext-GAIL* (?). This model addresses the task of procedure planning through reinforcement learning techniques. Similar to our approach, Ext-GAIL breaks down the procedure planning challenge into two distinct sub-problems. However, in Ext-GAIL, the primary objective of the first sub-problem is to supply extended horizon insights for the subsequent stage, whereas our primary intention is to establish conditions for the purpose of sampling.
- *P³IV* (?). P³IV constitutes a transformer-based model operating within a single branch, enhanced by an adaptable memory bank and an additional generative adversarial framework. Similar to our approach, P³IV also conducts simultaneous prediction of all action steps during the inference process.
- *PDPP* (?). PDPP formulates procedure planning as a distribution fitting problem. In this context, it characterizes the distribution of the complete intermediate action sequence using a diffusion model, effectively converting the planning problem into a sampling process from this distribution. It is worth noting that PDPP abstains from deploying resource-intensive intermediate supervision and instead leverages task labels sourced from instructional videos for guidance.

Table 1: Evaluation results of SR with protocol 2 on CrossTask. Prediction horizon is set to $T = \{3, 4, 5, 6\}$.

	$T=3$	$T=4$	$T=5$	$T=6$
P ³ IV	24.40	15.80	11.80	8.30
PDPP	53.06	35.28	21.39	13.22
Ours	55.54	37.03	24.22	14.97

C. Evaluation with another evaluation protocol

Beyond the evaluation protocol used in the main paper (thereafter called “Protocol 1”), previous works (???) have reported results on an alternative evaluation approach referred to as “Protocol 2”. It features a different train/test split strategy and a different sampling method with respect to the planning horizon. In particular, *a*) “Protocol 2” diverges in its data distribution, employing a partition of 2390 training samples and 360 testing samples. This distribution differs from “Protocol 1”, which adopts a 70%-train vs. 30%-test split, affixed with a sliding window technique to derive the training data. *b*) In “Protocol 2”, one procedure plan with a prediction horizon T is randomly chosen from each video for both training and testing purposes. This contrasts with “Protocol 1” that relies on a sliding window of size T to encompass all procedure plans within each video. *c*) “Protocol 2” modifies the prediction approach for a given planning horizon T , by restricting the prediction to encompass $T - 1$ actions, different from the prediction scope in “Protocol 1”.

In the evaluation under “Protocol 2,” we conduct a comparative analysis of our model’s performance against the results reported in prior studies on the CrossTask dataset. The comparison results are shown in Table 1. It is evident that our method consistently achieves the highest performance across all prediction horizons.

D. Influence of task classification

As demonstrated in our main paper, task classification accuracy can be enhanced by substituting the MLP with a Transformer. We reported the performance of our model using the Transformer model as task classifier. To dissect the effect of task classifier (MLP vs. Transformer), we compare the final action planning success rates (SR) using MLP and Transformer classifiers respectively within PDPP and our model in Table 2. The evaluation is done on the COIN dataset only, considering that the effect of task classification could be weaker on CrossTask and NIV datasets, because task classification accuracy is already quite high on these datasets. It is evident that when the task classifier’s performance improves, a corresponding enhancement can be observed in the final action planning SR for both PDPP and our models.

E. Influence of action searching space on procedure planning performance

One motivation of our masked diffusion is to deal with the large search space embodied by many action types. We anticipate the benefit of masking is more profound when the search space is larger. To validate this hypothesis, we manipulate the size of search space (i.e., number of action

Table 2: Comparison results (SR \uparrow) between using MLP and Transformer as the task classifier for PDPP and our model. The value in the bracket is the task classification accuracy.

Model	Classifier	$T = 3$	$T = 4$
PDPP	MLP	21.33 (0.810)	14.41 (0.802)
	Transformer	21.93 (0.826)	15.03 (0.819)
Ours	MLP	27.85 (0.810)	20.24 (0.802)
	Transformer	29.43 (0.826)	21.03 (0.819)

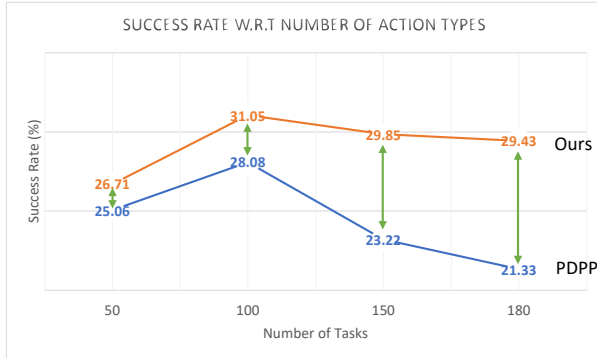


Figure 2: Success rate comparison between PDPP and our method with different numbers of action types. Evaluated on the COIN dataset with the planning horizon $T = 3$

types) and compare the performance (using SR as the metric) of PDPP and our method. In our method, we use the MLP model for task classification as in PDPP to ensure that the performance differences are attributed to the usage of masked diffusion. In other words, we show if masking (our method) lead to higher performance gap compared to not using masking (PDPP) when handling larger search spaces. In implementation, we randomly extract 50, 100, and 150 tasks from the full COIN dataset (comprising 180 tasks) to create three distinct subsets. By increasing the number of tasks, the number of action types also increase. Subsequently, we subject these subsets to evaluation using both our model and PDPP. The SR results of the two methods with a planning horizon of 3 are shown in Figure 2. It is evident that the performance advantage of our method over PDPP becomes more profound as the number of tasks/action types increase. When there are 50 different tasks, our model demonstrates a marginal performance improvement of just 1.65% over PDPP. When the number of tasks increases to 100, the performance gain becomes 2.97%. Further extending the task number to 150, our model exhibits a substantial advantage with a margin of 6.63%. As shown in the main paper, our model outperforms PDPP by a significant margin of 8.10% in terms of SR on 180 task types on the full COIN dataset.

Please note that this experiment aims to demonstrate the performance gap trend between our method and PDPP as the number of tasks changes. It is important to understand that a method’s performance on various subsets might not consistently follow a trend due to potential biases introduced by randomly selecting tasks to form subsets. This helps explain the phenomenon that SR of both methods shows improve-

ment when applied to subsets with a task count ranging from 50 to 100. However, this trend reverses as the task count in subsets continues to increase to 100 and 150.

F. Uncertainty modeling on NIV and COIN datasets

In the main paper, we delve into an in-depth exploration of our model’s probabilistic modeling prowess on the CrossTask dataset. Our investigation highlights the capacity of our masked diffusion model to generate plans that are not only accurate but also possess a commendable degree of diversity. In this document, we extend our analysis by offering comprehensive insights, presenting additional results of our model’s ability to handle uncertainty.

We adhere to the protocol in (?) to evaluate uncertainty and diversity. In the case of the Deterministic baseline, a single sampling process suffices to generate the plan, given that the outcomes are certain when observations and task class conditions are provided. For the Noise baseline, the PDPP diffusion model, and our masked diffusion model, we sample 1,500 action sequences to derive our probabilistic outcomes for the computation of uncertainty metrics. Since the computational load is high, we employ the DDIM sampling method (?) to accelerate the sampling procedure within the PDPP diffusion model and our masked diffusion model.

We present the uncertainty modeling results on NIV (Table 3, Table 4) and COIN (Table 5, Table 6), as an extension to that on the CrossTask dataset (presented in the main paper). The results on NIV show a striking similarity to those on CrossTask dataset. Specifically, both the PDPP and our approach exhibit a positive impact on the NIV dataset. In that sense, our method consistently demonstrates a superior capability in capturing uncertainty within procedure planning. The results also indicate that our method consistently excels in generating plans that exhibit a harmonious blend of diversity (measured by $KL-Div$ and NLL) and rationality (measured by SR , $Prec$ and Rec) across both prediction horizons.

On the COIN dataset, it is reported (and replicated in our experiment) that the PDPP method had a detrimental effect on performance (?). This is indicated by the larger values of both Kullback-Leibler Divergence ($KL-Div$) and Negative Log Likelihood (NLL), which is inferior to the Deterministic method. Furthermore, the PDPP approach yields diminished values for Success Rate (SR), mode Precision ($Prec$), and mode Recall (Rec) compared to the deterministic approach. The divergent performance of the PDPP method across datasets is assumed to stem from disparities in data scales and the inherent variability present in goal-conditioned plans within each dataset (?). In other words, given the substantial scale of the COIN dataset, the diffusion model encounters difficulties in effectively accommodating its intricacies. The introduction of noise to the model increases the difficulties of learning rather than alleviating them. In contrast, our masked diffusion model introduces noise solely within the confines of the task-defined subset. As a result, the search space for optimal actions is significantly narrowed when compared to the entirety of the dataset’s action space.



In the image, a person is pouring a mixture into a measuring cup. The person is likely preparing a recipe that requires measuring ingredients accurately.

pouring a mixture into a measuring cup.

Make Jello Shots-pour water.



In the image, a person is preparing a recipe by pouring ingredients into a bowl, which is placed on a table. The person appears to be focused on measuring and mixing the ingredients to create a dish.

preparing a recipe by pouring ingredients into a bowl.

Make Jello Shots-pour jello powder.



In the image, a person is pouring a yellow liquid, likely a drink or a sauce, into a bowl or measuring cup.

pouring a yellow liquid.

Make Jello Shots-pour juice.



In the image, a woman is shown putting air in her tire using an air compressor.

shown putting air in her tire using an air compressor.

Change a Tire-start loose.



In the image, a woman is kneeling down and attending to a flat tire on a car. She is either fixing the tire, changing it, or having someone help her with the process.

kneeling down and attending to a flat tire on a car.

Change a Tire-jack up.



In the image, a woman is jacking up a car's passenger side tire, likely to change it or perform some maintenance.

jacking up a car's passenger side tire.

Change a Tire-withdraw wheel.



In the image, a person is opening a coffee maker and pour water into it.

opening a coffee maker and pour water into it.

Make a Latte-pour water.



In the image, a person is adding coffee into a coffee maker.

Adding coffee into a coffee maker.

Make a Latte-add coffee.



In the image, a person is pouring a liquid, possibly a sauce or a drink, from a container.

Pouring a liquid.

Make a Latte-pour milk.



In the image, a person is pouring sugar onto a bowl full of strawberries.

pouring sugar onto a bowl full of strawberries.

Make French Strawberry Cake-add sugar.



In the image, a person is adding ingredients to a bowl on a table, using a spoon to mix the contents.

adding ingredients to a bowl on a table.

Make French Strawberry Cake-add butter.



In the image, a person is placing a generous amount of whipped cream on top of a dessert, which appears to be a pastry or a slice of cake.

placing a generous amount of whipped cream on top of a dessert.

Make French Strawberry Cake-spread creme upon cake.

Figure 3: Visualization of text-based action representations generated by LLaVA (?). Black captions represent direct outputs generated by LLaVA using prompts, while blue captions denote extracted keywords, and red captions correspond to the ground truth task and action.

Table 3: Evaluation results of the plan distributions metrics on NIV.

	$T=3$		$T=4$	
	KL-Div↓	NLL↓	KL-Div↓	NLL↓
Deterministic	5.40	5.49	5.13	5.26
Noise	4.92	5.00	5.04	5.17
PDPP	4.85	4.93	4.62	4.75
Ours	4.49	4.56	4.54	4.51

Table 4: Evaluation results of diversity and accuracy metrics on NIV.

	$T=3$			$T=4$		
	SR↑	Prec↑	Rec↑	SR↑	Prec↑	Rec↑
Deterministic	27.94	29.63	27.44	25.43	26.64	24.08
Noise	25.73	26.87	38.37	22.84	23.05	31.89
PDPP	31.25	31.78	33.09	26.72	29.10	33.08
Ours	32.35	31.93	40.58	28.88	29.63	38.09

Table 5: Evaluation results of the plan distributions metrics on COIN.

	$T=3$		$T=4$	
	KL-Div↓	NLL↓	KL-Div↓	NLL↓
Deterministic	4.52	5.46	4.43	5.84
Noise	4.55	5.50	4.52	5.92
PDPP	4.76	5.71	4.62	6.03
Ours	4.03	4.98	3.92	4.32

As evidenced by the outcomes presented in Table 5, our masked diffusion model exhibits remarkable proficiency in capturing the intricacies of uncertainty. Notably, our model boosts the lowest values for both *KL-Div* and *NLL* metrics across both horizons. Regarding diversity and accuracy, the results are shown in Table 6. In terms of Success Rate (*SR*), our model demonstrates accuracy that is comparable to the Deterministic approach, with a marginal difference of 0.1% lower at $T = 3$, and a slightly superior performance at $T = 4$. Furthermore, a substantial enhancement in *SR* is evident in our model when compared to the PDPP model, with notable improvements of 6.6% at $T = 3$ and 5.8% at $T = 4$. In terms of *Prec*, our model achieves slightly lower values when compared to the Deterministic approach at both $T = 3$ and $T = 4$. However, our model still outperforms PDPP significantly, with a substantial margin of 4.74% at $T = 3$ and 5.51% at $T = 4$. For *Rec*, our model surpasses the performance of the Deterministic approach by a substantial margin, with improvements of approximately 14% at $T = 3$ and 11.4% at $T = 4$. Furthermore, compared to PDPP, the advantages of our model become even more evident, with notable margins of around 18% at $T = 3$ and 15% at $T = 4$. A higher value of *Rec* in our model indicates its ability to predict plans that encompass a greater number of ground truth modes.

G. Prompts designed for the VLM model

In our experiments, we tried to extract image captions with emphasis on human action using a VLM model (LLaVA)

Table 6: Evaluation results of diversity and accuracy metrics on COIN.

	$T=3$			$T=4$		
	SR↑	Prec↑	Rec↑	SR↑	Prec↑	Rec↑
Deterministic	27.96	34.35	27.40	19.98	30.65	19.63
Noise	18.49	25.67	29.82	12.58	22.55	19.32
PDPP	21.33	28.03	23.49	14.41	24.83	16.26
Ours	27.85	32.77	41.11	20.24	30.34	31.05

(?). The following prompts are randomly chosen given an image.

- Please describe human action in this image.
- What is the person doing in the image?
- What is the human action in this image?
- What is the purpose of the human in this image?
- What action is the person in the image currently engaged in?
- Can you infer the person's action from the image?

In Figure 3, we present visualized examples of text-based action representations generated by LLaVA, showcasing image-related extracted keywords alongside the corresponding ground-truth task-action pairs. From examples in the figure, noticeable resemblances can be observed either in terms of *verbs* or *nouns* between the ground-truth action and our extracted key words. Such semantic similarity could be translated into enhanced representation learning, which ultimately help to boost accuracy of action planning.